Nano Zinc Oxide-Based Impedimetric Humidity Sensor

A. Anusuya[1], S. Karthickprabhu[1*], M. Mahendran[1]

[1]Centre of Excellence in Materials Research and Energy Solutions, Department of Physics, Thiagarajar College of Engineering, Madurai, Tamil Nadu, India - 625 015.

Abstract:

The demand for humidity sensors has increased significantly due to their essential role in environmental monitoring and industrial process control. Precise humidity regulation is critical in applications such as climate control systems, household appliances, video recording equipment, storage facilities, paper manufacturing, food processing, tobacco handling, textile industries, and moisture-sensitive integrated circuit (IC) packaging. In the semiconductor industry, particularly during advanced wafer fabrication, continuous monitoring of moisture levels is indispensable to ensure device reliability and performance. In addition, humidity sensors are widely used in domestic environments for intelligent building management, automated microwave cooking systems, and smart laundry control, as well as in various medical and industrial applications.

The main objective of the present study is to develop a humidity sensor based on nanostructured ZnO using the AC impedance technique. Three different ZnO nanomaterials were investigated: (i) a sputtered ZnO thin film with a thickness of approximately 100 nm, (ii) a commercially available ZnO powder with particle sizes below 100 nm, and (iii) an annealed form of the commercial ZnO powder. A detailed characterization of the samples was carried out employing X-ray diffraction (XRD), atomic force microscopy (AFM), UV–visible spectroscopy, Fourier transform infrared (FTIR) spectroscopy, Raman spectroscopy, and photoluminescence (PL) spectroscopy to assess their structural, morphological, and optical features.

Keywords: Humidity sensor; ZnO; Sputtering

1. Introduction:

Humidity refers to the amount of water vapor present in air or in a gas medium, whether it is a gas mixture such as air or a pure gas such as nitrogen or argon. Measurement of humidity is essential for determining the moisture content in these gaseous environments. In recent times, humidity has become a critical parameter in various industrial and agricultural processes, in the conservation of artworks and cultural heritage, and in many aspects of daily life. Since humidity is a constant environmental factor, its monitoring and regulation are vital not only for human comfort but also for the proper functioning of numerous industrial systems and technologies [1].

In the automotive sector, humidity sensors are employed in applications such as rear-window defogging systems and engine assembly lines. In the medical field, they are widely used in respiratory devices, sterilization systems, incubators, pharmaceutical manufacturing, and the handling of biological products. In agriculture, humidity sensors support greenhouse climate control, crop protection (including dew prevention), soil moisture assessment, and grain storage. Across general industrial applications, they play an important role in humidity regulation for chemical gas purification, drying systems, ovens, film drying processes, paper and textile manufacturing, and food processing operations. Applications in each field require different operating conditions.

Humidity sensors are divided into two main types viz. relative humidity sensors and absolute humidity sensors. Based on working principle or sensing element, humidity sensors can also be classified into two types i.e., resistive or capacitive type. In resistive type sensors, the DC resistance of the sensor varies with respect to the relative humidity level whereas in capacitive type sensor, the impedance of the sensor film changes with respect to the humidity level [2, 3].

2. Experimental details:

2.1 Chemicals:

Metallic zinc of 99.99 % purity with 50.8 mm diameter (Kurt J. Lesker Company, USA) was used as the solid target. Commercial zinc oxide nanopowder was purchased from ALDRICH chemicals for making the pellet. Analytical grade acetone (Merck), ethanol (S. D's), hydrochloric acid, sodium chloride, calcium chloride (all Qualigens), calcium nitrate, cupric chloride, potassium chloride (S. D's), and potassium acetate (CDH), potassium sulfate (Nice chemicals) and magnesium chloride (Fischer) were used. A microscopic glass slide with thickness of 1.35 mm was used as the substrate. Silicon substrate was procured from Chemplast Sanmar, India. Conductive silver paste was purchased from CH Instruments, USA. Double-distilled water was used to prepare the saturated salt solutions.

2.2 Preparation of ZnO samples:

A ZnO thin film with a thickness of 100 nm was deposited onto an etched glass substrate using the sputtering technique. High-purity argon served as the sputtering gas, while oxygen was introduced as the reactive gas. An argon–oxygen gas mixture in a 1:1 ratio was supplied at a total flow rate of 10 sccm, controlled by mass flow controllers. Prior to deposition, the chamber was evacuated to a base pressure of 8×10^{-6} mbar, and the working pressure during sputtering was maintained at 1×10^{-3} mbar. The target-to-substrate distance was fixed at 10 cm. A discharge current of 0.18 A was applied, corresponding to a discharge voltage of 375 V. During deposition, the substrate temperature was held at 300 °C to enhance the crystallinity of the film.

Its deposition was stopped when the thickness value in the digital thickness monitor attained 100 nm. The 100 nm ZnO film will be designated henceforth as Sample 1 respectively. About 200 mg of commercial ZnO nanopowder was used to make a pellet of diameter 1.2 cm which is designated as Sample 2. Sample 3 corresponds to a pellet made from an annealed commercial sample. annealing temperature was maintained at 300°C for 3 h. The sputtered film

and commercial powder samples (Table 1) were characterized for their structural, morphological, and optical properties and the results are presented below.

Table I: SAMPLE NOMENCLATURE

Sample Name	Sampling details
Sample 1	100nm thickness of ZnO film
Sample 2	Commercial ZnO powder
Sample 3	Commercial ZnO powder annealed at 300°C for 3h

2.3 Humidity sensor fabrication:

A custom-built glass chamber equipped with a sensor holder was employed to maintain controlled relative humidity (%RH) conditions. Specific %RH environments of 23, 32, 51, 67, 75, 84, and 97 at 30 °C were achieved using saturated aqueous solutions of potassium acetate, magnesium chloride, calcium nitrate, copper chloride, sodium chloride, potassium chloride, and potassium sulfate, respectively [4]. Prior to impedance measurements, each saturated salt solution was allowed to equilibrate inside the chamber for 24 h. A low-humidity condition of 6.3% RH was produced using anhydrous calcium chloride flakes [5], which was used to stabilize the sensor response before recording impedance data at each humidity level.

3. Results and Discussion:

3.1 X-ray diffraction:

In Fig 1, the XRD spectra for the commercial ZnO powder (Sample 2) and the annealed ZnO powder samples (Sample 3). For Samples 2 and 3, the XRD spectra (Fig. 1 (a) & (b)) show eleven diffraction peaks assigned to the lattice planes (100), (002), (101), (102), (110), (103), (200), (112), (201), (004) and (202) equivalent to the peak positions indicated in Table 2 & 3. The calculated lattice constants (d) and grain size are also shown. The d values of Samples 2 and 3 obtained from the observed XRD pattern (Tables 2 & 3) and the standard d values for ZnO (JCPDS File no: 36-1451) are compared. The experimental values are in decent arrangement through the standard d values. The following significant observations can be made with regard to the XRD data: (a) The estimated lattice constants of the ZnO Samples 2 and 3 compare well with the standard values. (b)

The ZnO powder sample (both unannealed and annealed) is highly polycrystalline. (c) The average grain size as calculated using the Debye-Scherer formula is about 44.8 nm for Sample 2 and 41.6 nm for Sample 3. (d) The XRD spectrum of Sample 3 is qualitatively analogous to that of Sample 2 representing that the commercial sample is of high purity. However, some modifications can also be observed between the two samples' XRD spectrum. (e) For example, the crystal orientation is changed on annealing in that while (100) is the most prominent peak in Sample 2, it is (101) for Sample 3. Further, annealing has a notable influence on the FWHM values especially for the peaks with larger 2theta values. As seen from Table 3 for Sample 3, the diffraction peak with hkl index (202) for which the FWHM is considerably decreased, the crystallite size is increased to almost twice the value obtained for that of the same lattice plane in the unannealed sample. The relative intensity values of the (202) peak is 2.26 % and 3.6 % for the unannealed and annealed samples respectively. This helps to infer that the crystallinity of the material is slightly better in the annealed sample [3-6]. The XRD findings closely correspond to the JCPDS File no: 36-1451.

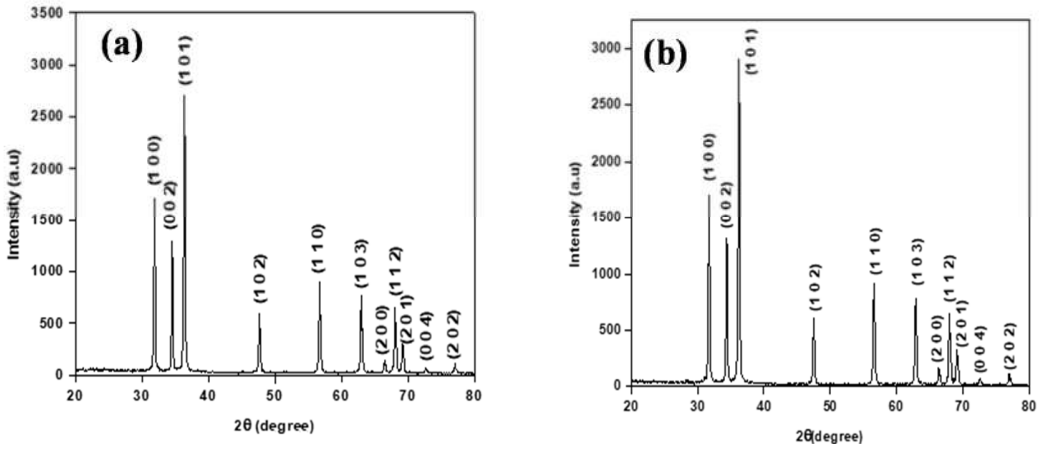

Fig. 1 XRD spectra of (a) unannealed commercial ZnO powder and (b) ZnO powder annealed at 300°C for 3 h.

Table II: Lattice parameter and grain size for Sample 2

Position (2θ)	FWHM (2θ)	d spacing (Å)	(h k l)	Estimated lattice constants (Å)	Grain size (nm)
31.85	0.18	2.80	100		
34.50	0.16	2.59	002		
36.33	0.19	2.47	101		
47.61	0.20	1.90	102		
56.66	0.19	1.62	110		

62.92	0.18	1.47	103	a = 3.24	44.88
66.44	0.19	1.40	200	c = 5.20	
68.01	0.18	1.37	112		
69.14	0.19	1.35	201		
72.63	0.40	1.30	004		
77.01	0.47	1.23	202		

TABLE III. Lattice parameter and grain size for Sample 3

Position (2θ)	**FWHM (2θ)**	**d spacing (Å)**	**(h k l)**	**Estimated lattice constants (Å)**	**Grain size (nm)**
31.72	0.19	2.81	100		
34.37	0.17	2.60	002		
36.21	0.20	2.47	101		
47.49	0.20	1.91	102	a = 3.25	
56.55	0.20	1.62	110	c = 5.20	41.65
62.82	0.23	1.47	103		
66.34	0.26	1.40	200		
67.90	0.22	1.37	112		
69.04	0.23	1.35	201		
72.52	0.58	1.30	004		
76.92	0.19	1.23	202		

3.2 Atomic force microscopy (AFM):

Figs 2 - 4 shows the 2-D, 3-D and roughness profiles for the Samples 1 to 3 respectively. The cluster size and the roughness results are shown in the Table 4. The AFM images for Samples 2 (Fig. 3) and 3 (Fig. 4) were obtained by casting the ZnO dispersion on a clean glass plate. The ZnO dispersion was prepared by sonicating ZnO powder in double-distilled water for 1 hour. The AFM of Sample 2 shows spherical nanoparticles with an average cluster size of 40 nm, whereas for Sample 3, the image shows somewhat large spherical particles of size 113 nm due to the annealing effect. The 3-D images of both Sample 2 and Sample 3 suggest a porous morphology. The roughness of Sample 3 is lesser than that of Sample 2.

Among the three samples, Sample 2 (commercial powder) shows the smallest particle size and maximum surface roughness among the three samples. For gas sensor application, the high surface roughness will provide a high surface-to-volume ratio thereby enhancing the chemical active area of the film [6].

TABLE IV. Particle size and roughness measurement from AFM

`Sample	Particle size (nm)	Roughness (nm)
1	165	2.61
2	40	3.2
3	113	1.7

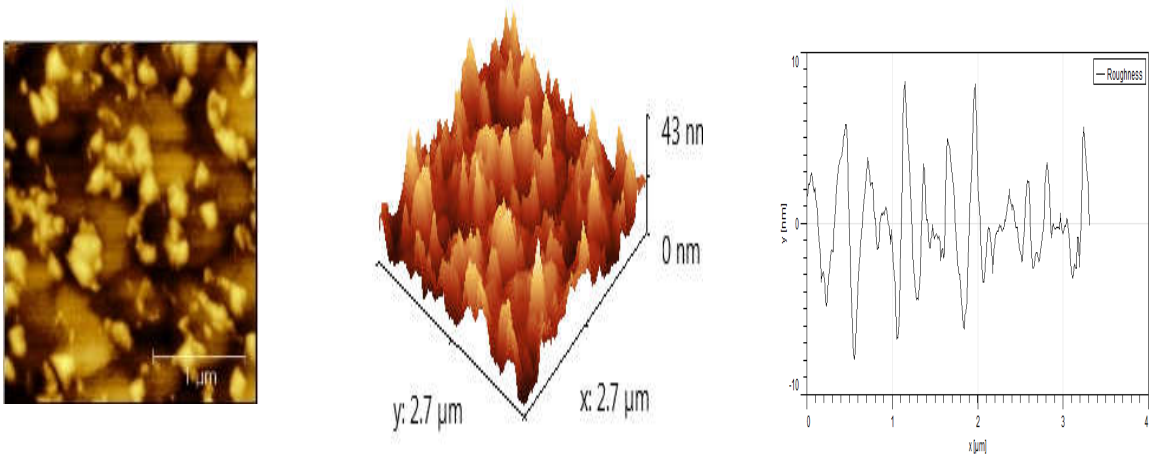

Fig. 2 AFM image of sample 1 a) 2-D image b) 3-D image c) roughness plot

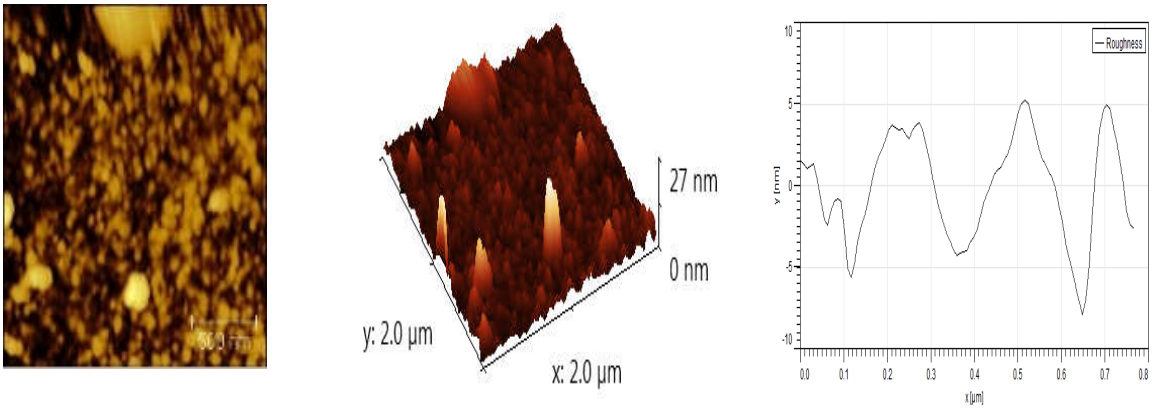

Fig. 3 AFM image of sample 2 a) 2-D image b) 3-D image c) roughness plot

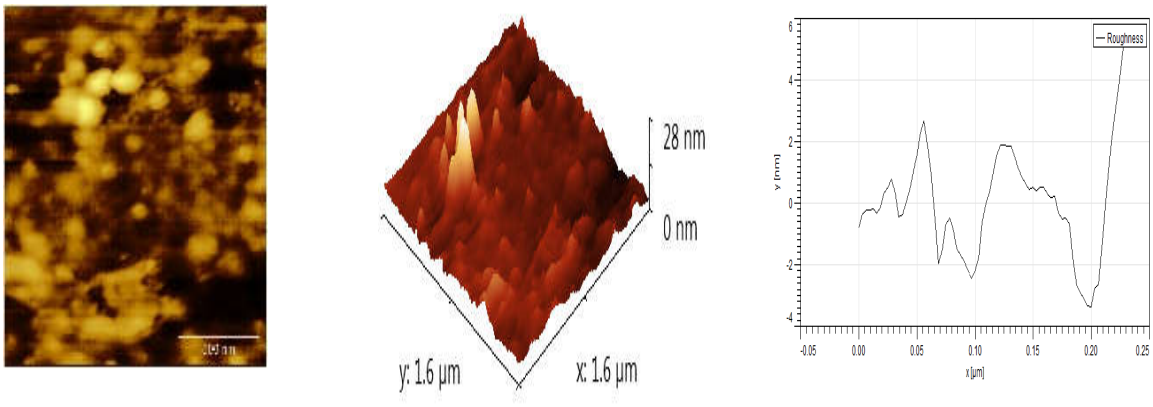

Fig. 4 AFM image of sample 3 a) 2-D image b) 3-D image c) roughness plot

3.3 Absorption spectral data:

Fig.5 shows a absorption spectra for the three ZnO Samples. For sample 1 also, the spectrum shows a broad absorption peak but at a higher wavelength value of about 362 nm. This is perhaps attributable to the larger grain size in Sample 1. However, these values are significantly lower compared to the reported value of 380 nm for the bulk ZnO sample [7]. The remarkable blue shift of the absorption maximum is suggestive of a great reduction of its size for the ZnO particles presence in its sputtered films. The bandgap value of Sample 1 has been estimated to be 3.26 eV by the extrapolation of the linear portion of $(\alpha h\nu)2$ vs (eV) plot to $\alpha = 0$ as exposed in the insert of Figs. 5 (a) and (b) where α is the absorption coefficient obtained from Eq. 1 [8].

$$\alpha = 2.303\ A/d \qquad (1)$$

in which A is the absorbance and d is the thickness of the film. The observation of a reduced band gap in the sputtered ZnO film relative to bulk ZnO (3.37 eV) is somewhat unexpected, particularly in view of the smaller grain size of the deposited film. Nevertheless, similar red shifts in the band gap of nanostructured ZnO have been reported in the literature and are commonly associated with the presence of intrinsic defects, including zinc interstitials and oxygen vacancies [9–11].

Fig.5 (b) shows the absorption spectra of Sample 2 and Sample 3. The spectra of the two powder samples (commercial sample and its annealed form) have the same absorption maximum of 376 nm. The results indicate that annealing does not affect the band gap values.

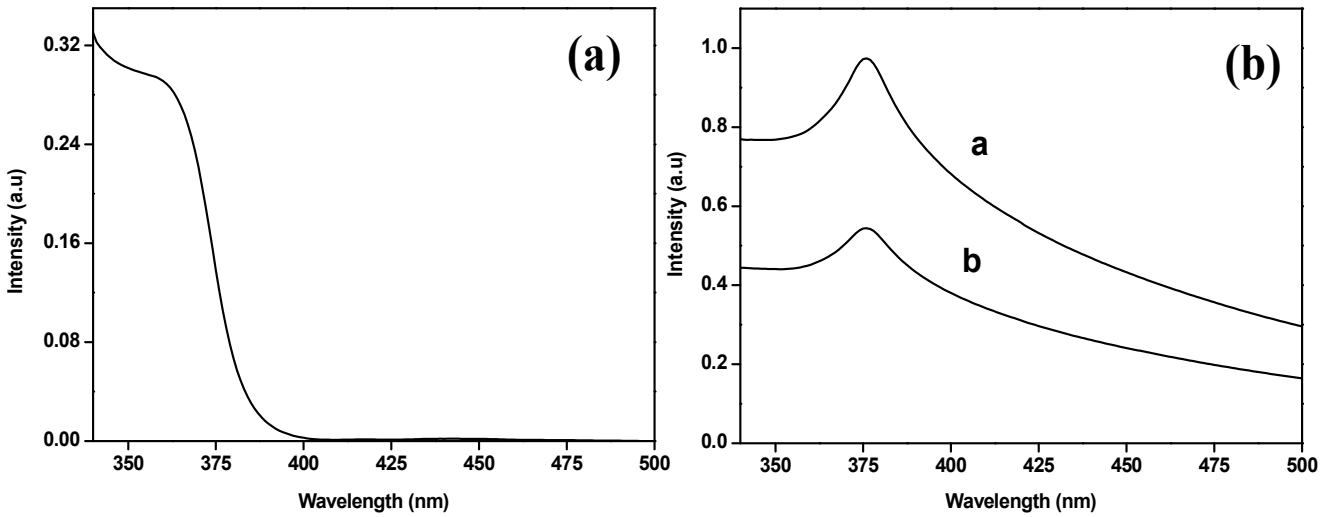

Fig. 5 UV- Visible spectrum. Inset shows the plot for the determination of band gap. (a) 100 nm ZnO film (b) a - unannealed and b – annealed ZnO powder

3.4 Fourier-transform infrared spectroscopy (FTIR):

FTIR spectroscopy confirmed the existence of ZnO in the sample. The film samples were sputter-deposited on a silicon substrate for this purpose [12]. The powder samples are hard-pressed into a pellet with KBr. Figure 6 presents the FTIR spectra of the three ZnO samples. In all cases, a strong absorption band appears near 410 cm^{-1}, which is attributed to the Zn–O stretching vibration [13–14]. The lack of additional characteristic peaks in the spectra indicates the high purity of the samples.

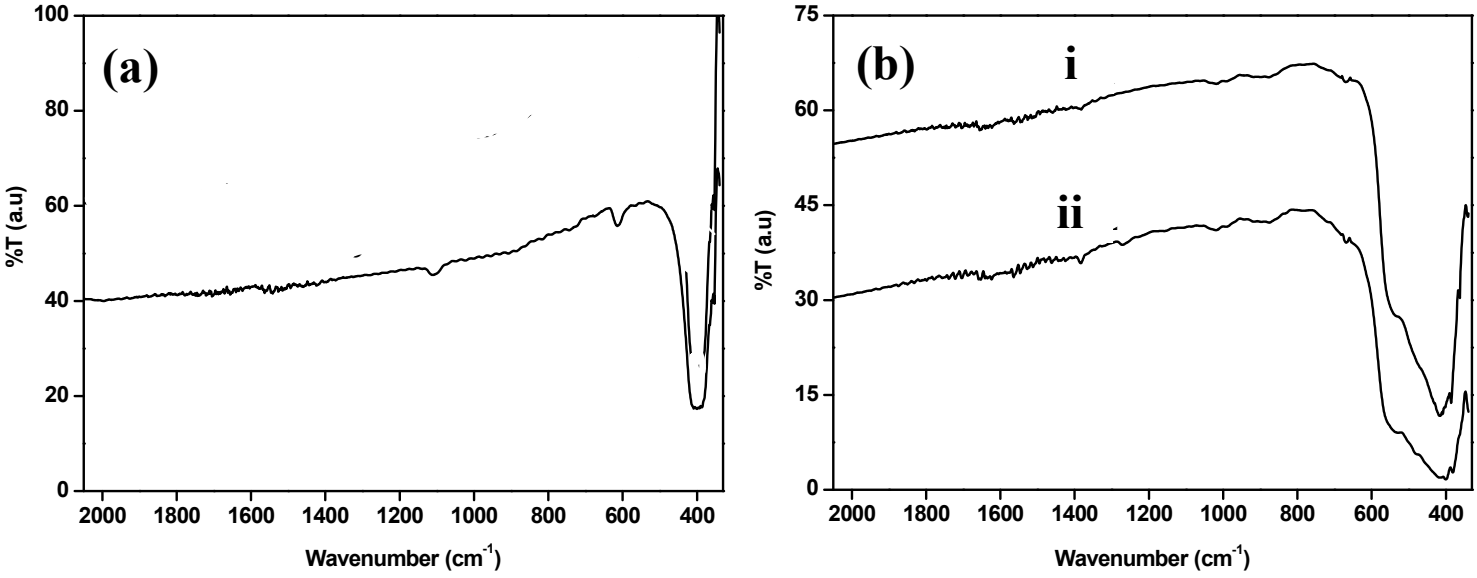

Fig. 6 FTIR spectrum a) 100 nm ZnO film b) (i) unannealed ZnO (ii) annealed ZnO

3.5 Raman spectroscopy:

The ZnO crystal's vibrational characteristics can be investigated by using Raman spectroscopy. In the space group C6v4, ZnO exhibits semiconducting behavior and possesses a wurtzite crystal lattice. Each primitive cell has two formula units, and all of the atoms are located in C3v sites [15, 16]. Group theoretical considerations predict the occurrence of the following modes:

$$\Gamma opt = A_1 + 2B_1 + 2E_2 \qquad (2)$$

Both A_1 and E_1 modes are polar in nature and are split into longitudinal optical ($A_1(LO)$, $E_1(LO)$) and transverse optical ($A_1(TO)$, $E_1(TO)$) components. In contrast, the nonpolar phonon modes with E_2 symmetry comprise two distinct vibrations at low and high frequencies, denoted as $E_2(Low)$ and $E_2(High)$, which originate from oscillations of the Zn sublattice and oxygen atoms, respectively. The B_1 modes are generally Raman inactive. All of these phonon modes are well established in the Raman spectra of bulk ZnO [17]. For bulk ZnO, the Raman-active phonon modes are observed at approximately 102 cm^{-1} ($E_2(Low)$), 379 cm^{-1} ($A_1(TO)$), 410 cm^{-1} ($E_1(TO)$), 439 cm^{-1} ($E_2(High)$), 574 cm^{-1} ($A_1(LO)$), and 591 cm^{-1} ($E_1(LO)$). In ZnO nanostructures, both polar

and nonpolar optical phonon modes have been reported to exhibit a red shift relative to the bulk values [18].

Fig. 7 displays the Raman spectra for Samples 1 to 3. The values of the experimental Raman frequencies are noted in Table 5 including the reported values for bulk ZnO. In the case of Samples 1, 303 cm^{-1} A1 (TO), 434 cm^{-1} E2 (High) and 571 cm^{-1} A1 (LO) are observed among which the prominent A1 (TO) mode is substantially red shifted from 379 cm^{-1} for bulk sample in alignment with the nanostructured form of the sample. Some 2nd order peaks have been displayed at about 943-983 cm^{-1} [19].

The Raman spectra of the unannealed and annealed samples are largely similar confirming again the good sample purity and also there is no major structural change during annealing. However, they are different from the Raman spectra of the film sample (Sample 1) in that the most intense peak is the sharp 434 cm-1 E2(High) mode. The Raman frequency at 330 cm^{-1} (A1(TO)) is somewhat increased and that is noted for Sample 1 but is red-shifted compared to the reported value for bulk ZnO due to the smaller grain size. Further, the broad band observed between 1060 and 1200 cm^{-1} can be attributed to multiphonon processes [20, 21].

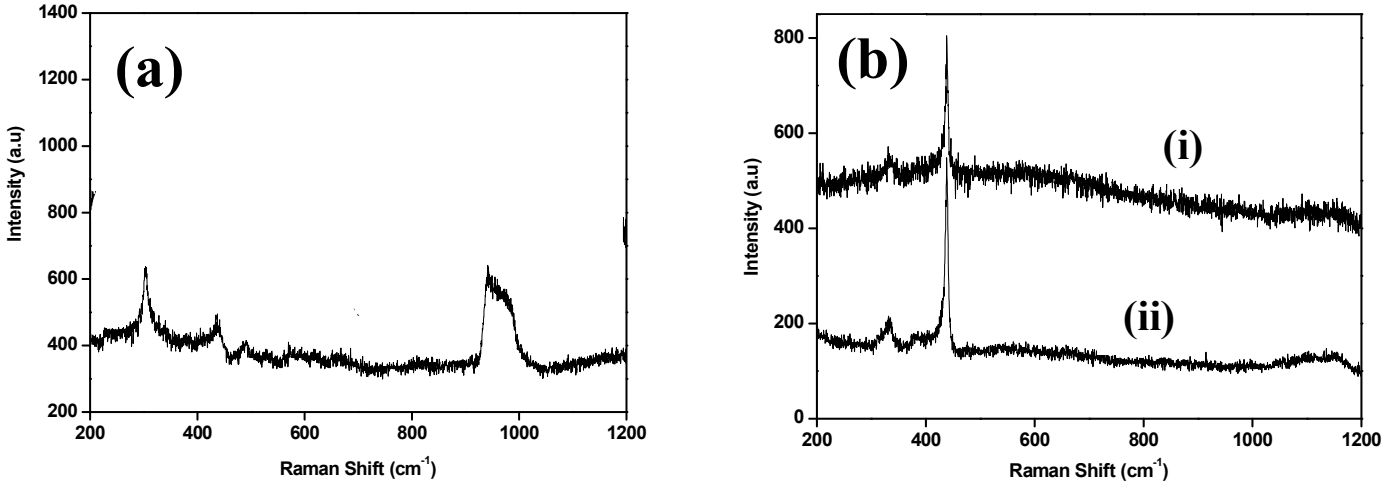

Fig. 7 Raman spectrum a) 100 nm ZnO film b) (i) annnealed (ii) unannealed ZnO powders

3.6 Photoluminescence (PL) studies:

The photoluminescence spectra corresponding to Samples 1, 2, and 3 are shown in Fig. 8. All the three samples show two characteristic peaks whose lmax values are indicated in Table 5. The peak in the UV region (351-382 nm) is ascribed to a near-band-edge emission that arises from the recombination of free excitons, whereas the broad emission observed in the green region (400–543 nm) is associated with deep-level transitions originating from structural defects such as interstitials and oxygen vacancies. The PL spectra of the three samples show notable differences. The PL spectrum of Sample 1 shows only a shoulder peak at 361 nm and also the green peak is blue shifted considerably to 400 nm with a reduced broadness. It is therefore inferred that Sample 1 has small structural defects. In the cases of the Samples 2 and 3, the spectra show one sharp peak at 381 and 382 nm. Further one wide peak in the green region at about 543 and 501 nm respectively. The presence of the prominent peaks at about 380 nm peak indicates that Samples 2 and 3 are highly crystalline. This observation also agrees very well with the inference from their XRD data as well.

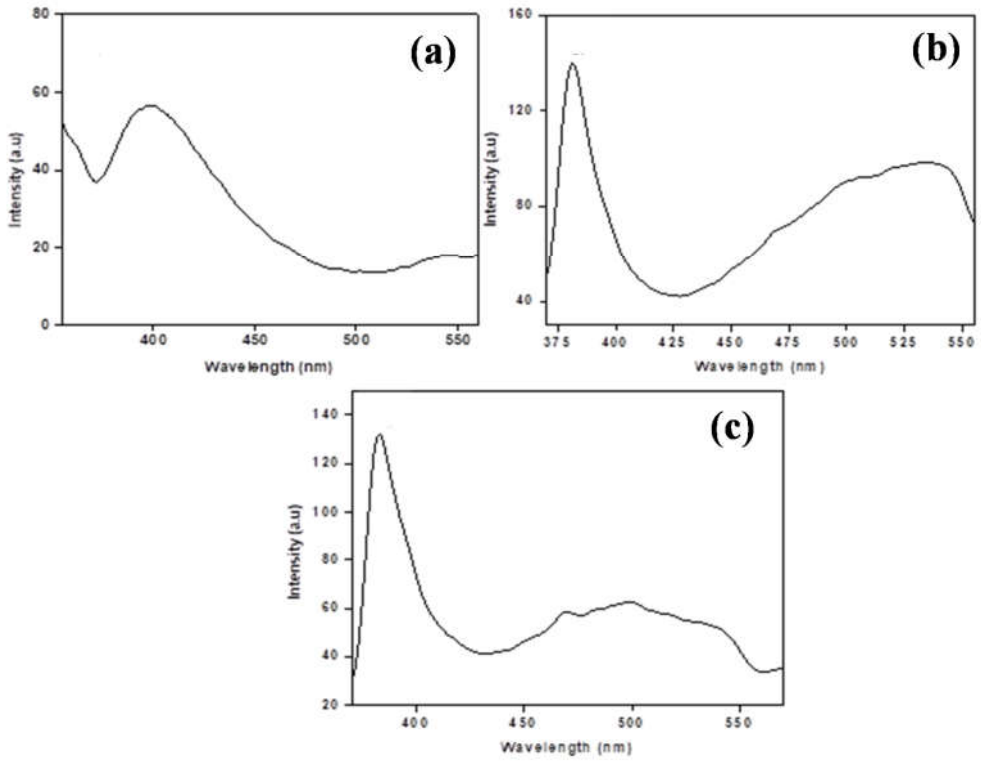

Fig. 8 Photoluminescence spectra at an excitation wavelength of 280 nm (a) 100 nm ZnO film (b) unannealed ZnO and (c) annealed ZnO

TABLE V. Emission peak values

`Sample	UV emission peak (nm)	Green emission peak (nm)
1	361	400
2	381	543
3	382	501

3.7 Humidity sensing response of Sample 2

Fig. 9 shows the impedance data of Sample 1 (100 nm sputtered film) at various % RH values. The plots are made in the frequency range between 1 KHz and 1 MHz except for 84 and 97 %RH in which cases, the Nyquist plots could be constructed in the entire frequency range of 1 Hz to 1 MHz. The general behavior have the semicircle which becomes more prominent with

increasing humidity levels. A second semicircle corresponding to the grain boundary effect is observed at 84 %RH. A Warburg impedance significant of diffusion can be noted at 97 %RH. An inductance loop is also observed at high frequency. The asymmetric broadening of the impedance curves suggests a change in relaxation in Sample 1. A two-order decrease in the relaxation time is observed when the humidity level is varied between 75 and 84 % RH (Table 6). Also, the impedance (Z''max) is somewhat larger for Sample 1, especially at lower humidity levels. This probably shows a grain growth, grain boundary and electrode interface resistance values as the film thickness gets increased. The impedance data for Sample 1 suggest that grain effects are more predominant than grain boundary and electrode effects

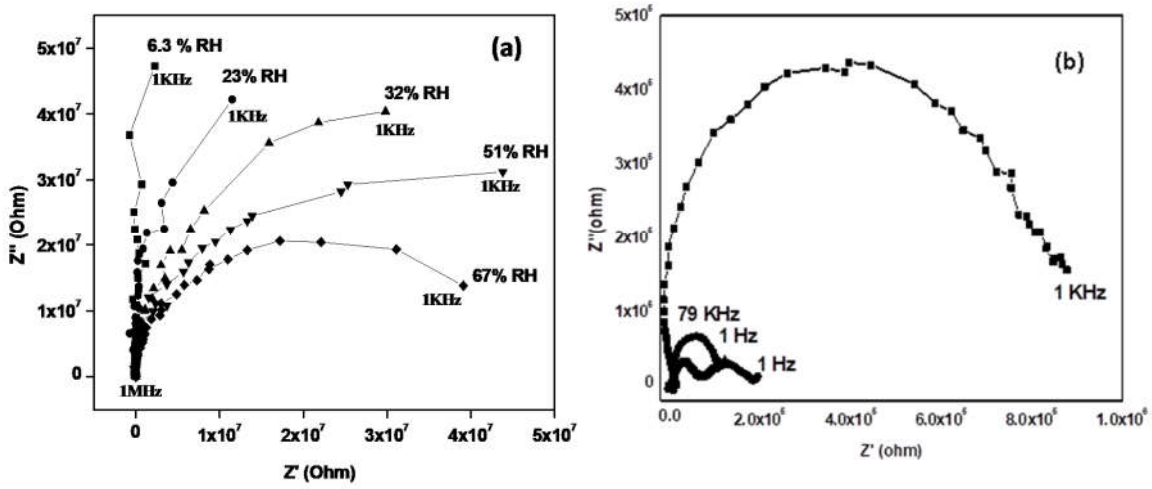

Fig. 9 (a) & (b) Complex impedance spectra of Sample 1 at various humidity levels

TABLE VI. Charge transfer resistance (RCT) and Relaxation time (τ) at different humidity levels for Sample 1

`% RH	RCT (KΩ)	τ (s)
6.3	-	-
23	-	-
32	-	-
51	-	-
67	-	-
75	13000	1×10^{-3}
84	89.5	1.26×10^{-5}
97	57	1×10^{-5}

4.

Conclusion:

The main objective of this research work is to develope a nanostructured ZnO based humidity sensor using AC impedance technique. Three ZnO samples have been evaluated for this purpose. Samples 1 is the 100 nm thin film prepared by the DC reactive magnetron sputtering technique. Sample 2 is a pellet made of the commercial ZnO powder and Sample 3 is also made of the commercial ZnO powder after annealing at 300oC for 3 h. The sputtered film and the commercial samples have been scientifically characterized through XRD, FTIR, UV-vis and Raman spectroscopy and photoluminescence measurements. The salient findings of the project are summarized below:

The XRD data of the Samples 2 and 3 have helped to infer that the ZnO has a wurtzite crystal structure with estimated lattice constants of a= b= 3.2 Å and c = 5.2Å. The commercial sample is more polycrystalline than the ZnO prepared by the DC reactive magnetron sputtering. Annealing of the commercial ZnO powder has resulted in a slight change of crystal orientation from (100) to (101) plane. There is a slight increase in crystallinity of the ZnO powder after annealing. The FT-IR spectra of all the three samples show the characteristic Zn-O stretching band at 410 cm^{-1}. The estimated ZnO cluster size from the AFM data are 165 nm, 40 nm and 113 nm for Samples 1 to 3 respectively. The crystal size of Sample 2, and its surface roughness is the highest among the three samples. The high surface roughness of Sample 2 can provide a high

surface-to-volume ratio thereby enhancing the active zone of the sample and thus the water vapor adsorption. Its band gap values of the ZnO sputtered film, Sample 1 is evaluated from the absorption spectral data as 3.26 eV. The absorption spectral result is highly same as for the samples 2 and 3 suggesting that the annealing process has not affected the energy band gap. The Raman spectral data show that the A1 (TO) phonon mode at 303 cm^{-1} is more prominent in the sputtered film sample while the E2(High) mode at 434 is more prominent in the commercial powder sample.

Photoluminescence spectral data have given valuable information on the defect levels in the three samples. A higher concentration of structural defects, including interstitials and oxygen vacancies, is expected to enhance the interaction between adsorbed water molecules and the surface of the sample1. It is interesting that Sample 1 shows a good response only at humidity levels greater than 67 %.

Acknowledgments

The Thiagarajar Research Fellowship (TRF) scheme contributed financial support for this research work (Grant No: TCE/RD/TRF/Jan-2024/01).

References

[1] M. Bayhan, T. Hashemi, & A. Brinkman, “Sintering and humidity-sensitive behaviour of the ZnCr2O4–K22CrO4 ceramic system” Journal of Materials Science 32, 6619–6623 (1997). https://doi.org/10.1023/A:1018692101445.

[2] Wang, W; Li, Zhenyu; Liu, L; Zhang, H; Zheng, W; Wang, Y; “Humidity sensor based on LiCl-doped ZnO electrospun nanofibers” Sens. Actuators, B 141, 404, Journal contribution. (2009). https://hdl.handle.net/10536/DRO/DU:30048185

[3] M.E.V. Costa, P.Q. Mantas, J.L. Baptista, “Effect of electrode alterations on the a.c. behaviour of Li2O・ZnO humidity sensors” Sensors and Actuators B: Chemical, Volume 27, Issues 1–3, Pages 312-314, ISSN 0925-4005, 1995, https://doi.org/10.1016/0925-4005(94)01608-K.

[4] Rockland, L. B."Saturated Salt Solutions for Static Control of Relative Humidity between 5° and 40° C", Analytical Chemistry,32,10, 1375-1376, 1960, https://doi.org/10.1021/ac60166a055.

[5] Milind V. Kulkarni, Annamraju Kasi Viswanath, P.K. Khanna, “Synthesis and humidity sensing properties of conducting poly(N-methyl aniline) doped with different acids”, Sensors and Actuators B: Chemical, Volume 115, Issue 1, 2006,Pages 140-149,ISSN 0925-4005, https://doi.org/10.1016/j.snb.2005.08.031.

[6] Farmakis, Th. Speliotis, K.P. Alexandrou, C. Tsamis, M. Kompitsas, I. Fasaki, P. Jedrasik, G. Petersson, B. Nilsson, “Field-effect transistors with thin ZnO as active layer for gas sensor applications, Microelectronic Engineering”, Volume 85, Issues 5–6, Pages 1035-1038, 2008, https://doi.org/10.1016/j.mee.2008.01.040.

[7] Srikant, V, Clarke, D. R."On the optical band gap of zinc oxide", Journal of Applied Physics, VO 83, IS 10, YR 1998, https://doi.org/10.1063/1.367375

[8] Sahay, P.P., Tewari, S. and Nath, R.K. “Optical and electrical studies on spray deposited ZnO thin films” Cryst. Res. Technol., 42: 723-729. (2007), https://doi.org/10.1002/crat.200610895

[9] Lu, Xi-Hong, Wang, Dong,Li, Gao-Ren, Su, Cheng-Yong, Kuang, Dai-Bin, Tong, Ye-Xiang, “Controllable Electrochemical Synthesis of Hierarchical ZnO Nanostructures on FTO Glass”, The Journal of Physical Chemistry C, American Chemical Society, VL - 113, SP - 13574, EP - 13582, 2009, https://doi.org/10.1021/jp902834j

[10] X.C. Wang, X.M. Chen, B.H. Yang,"Microstructure and optical properties of polycrystalline ZnO films sputtered under different oxygen flow rates", Journal of Alloys and Compounds, Volume 488, Issue1,Pages232-237,2009, https://doi.org/10.1016/j.jallcom.2009.08.089.

[11] F Chaabouni, M Abaab, B Rezig,"Effect of the substrate temperature on the properties of ZnO films grown by RF magnetron sputtering", Materials Science and Engineering: B, Volume 109, Issues 1–3,Pages 236-240, 2004, https://doi.org/10.1016/j.mseb.2003.10.105.

[12] Chennupati Jagadish and Stephen J. Pearton,"Zinc oxide bulk, thin films and nanostructures : processing, properties and applications" 2006, https://api.semanticscholar.org/CorpusID:92960322

[13] S. K. Nandi, S. Chakraborty, M. K. Bera and C. K. Maiti, "Structural and Optical Properties of ZnO Films Grown on Silicon and Their Applications in MOS Devices in Conjunction with ZrO2 as a Gate Dielectric," Bulletin of Materials Science, Vol. 30, No. 3, 2007, pp. 247-254. doi:10.1007/s12034-007-0044-3

[14] Kwon, Y.J., Kim, K.H., Lim, C.S. and Shim, K.B. (2002) Characterization of ZnO nanopowders synthesized by the polymerized complex method via an organochemical route. J Ceram Process Res, 3, 146-149.

[15] Arguello, C. A. and Rousseau, D. L. and Porto, S. P. S."First-Order Raman Effect in Wurtzite-Type Crystals"Phys. Rev., volume 181,issue 3, year 1969, American Physical Society, pages 1351--1363, https://link.aps.org/doi/10.1103/PhysRev.181.1351

[16] Lo SS, Huang D. "Morphological variation and Raman spectroscopy of ZnO hollow microspheres prepared by a chemical colloidal process", Langmuir. 2010; 26(9):6762-6. doi: 10.1021/la904112j. PMID: 20146484.

[17] Rui Zhang, Peng-Gang Yin, Ning Wang, Lin Guo, "Photoluminescence and Raman scattering of ZnO nanorods", Solid State Sciences, Volume 11, Issue 4, Pages 865-869,2009, https://doi.org/10.1016/j.solidstatesciences.2008.10.016.

[18] Khan A. Alim, Vladimir A. Fonoberov, Manu Shamsa, Alexander A. Balandin; Micro-Raman investigation of optical phonons in ZnO nanocrystals. J. Appl. Phys. 15 June 2005; 97 (12): 124313. https://doi.org/10.1063/1.1944222

[19] I. Calizo, K. A. Alimb, V. A. Fonoberova, S. Krishnakumar, M. Shamsa ,A. A. Balandin and R. Kurtz, “Micro-Raman spectroscopic characterization of ZnO quantum dots, nanocrystals, and nanowires”Proceedings Volume 6481, Quantum Dots, Particles, and Nanoclusters IV; 64810N (2007) https://doi.org/10.1117/12.713648.

[20] Qi Qi, Tong Zhang, Qingjiang Yu, Rui Wang, Yi Zeng, Li Liu, Haibin Yang, "Properties of humidity sensing ZnO nanorods-base sensor fabricated by screen-printing", Sensors and Actuators B: Chemical, Volume 133, Issue 2,Pages 638-643, 2008, https://doi.org/10.1016/j.snb.2008.03.035.

[21] J. M. Calleja, M. Cardona, “Resonant Raman scattering in ZnO” Phys. Rev. B 16 (1977) 3753, https://doi.org/10.1103/PhysRevB.16.3753.